Fuel 274 (2020) 117804

Contents lists available at ScienceDirect

Fuel

journal homepage: www.elsevier.com/locate/fuel

Full Length Article

Low pressure conversion of CO_2 to methanol over Cu/Zn/Al catalysts. The effect of Mg, Ca and Sr as basic promoters

D. Previtali[a], M. Longhi[b], F. Galli[c,*], A. Di Michele[d], F. Manenti[a], M. Signoretto[e], F. Menegazzo[e], C. Pirola[b]

[a] Dipartimento di Chimica, Materiali e Ingegneria Chimica "Giulio Natta", Politecnico di Milano, piazza Leonardo da Vinci 32, 20133 Milano, Italy
[b] Dipartimento di Chimica, Università degli Studi di Milano, via Golgi 19, 20133 Milano, Italy
[c] Department of Chemical Engineering, Polytechnique Montréal, C.P. 6079, Succ. CV, Montréal H3C 3A7, Québec, Canada
[d] Dipartimento di Fisica e Geologia, Università degli Studi di Perugia, via Pascoli 1, 06123 Perugia, Italy
[e] Dipartimento di Scienze Molecolari e Nanosistemi, Università Ca' Foscari Venezia, via Torino 155, 30170 Venezia Mestre, Italy

GRAPHICAL ABSTRACT

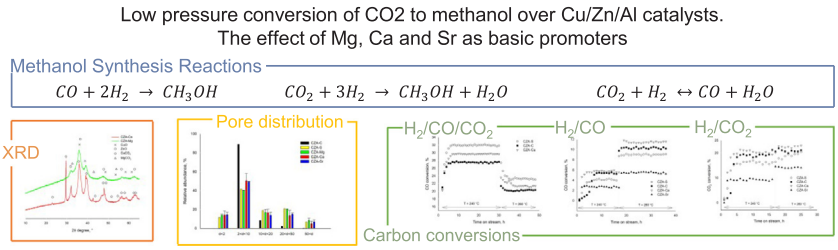

ARTICLE INFO

Keywords:
Methanol
CZA
Ca doped CZA
CO_2
Low pressure

ABSTRACT

Carbon dioxide concentration level is reaching a non-returning point. Carbon capture technologies are immature and short-term actions are necessary. The conversion of CO_2 into methanol is a technical challenge. Commercial copper-zinc-alumina catalysts convert maximum 7% carbon dioxide in syngas at high pressures (5 MPa to 10 MPa) and moderate temperatures (473 K to 573 K) into methanol. However, there are not records on the synthesis of methanol at low pressure ($P < 2.5$ MPa) and without a large excess of hydrogen in the feed. Here, we tested three new catalysts prepared by co-precipitation of copper, zinc and aluminum nitrates (CZA), with strontium, magnesium or calcium as basic promoters to enhance CO_2 conversion to methanol. We discussed the microstructure of the catalysts according to the supersaturation of the relative carbonates formed during the co-precipitation synthesis. Compared to the benchmark, the sample doped with Ca showed higher carbon conversion with all the feed compositions tested (syngas, synthetic biosyngas and CO_2 with H_2). CZA doped with Sr is inactive in this reaction.

1. Introduction

In December 2015, at the Paris United Nations Framework Convention on Climate Change (UNFCCC), 195 nations agreed to take action to stop global warming. The goal is to decrease the average temperature 2 K above the value at the pre-industrial level. This target is ambitious, yet feasible [1]. There is 66% chance to reach the objective if CO_2 quantity in atmosphere reduces by 1000Gt compared to 2011. Thanks to the exponential increase in wind and solar energy deployment [2] green electricity will be available at a competitive cost,

* Corresponding author.
E-mail address: federico.galli@polymtl.ca (F. Galli).

https://doi.org/10.1016/j.fuel.2020.117804
Received 21 October 2019; Received in revised form 27 March 2020; Accepted 6 April 2020
Available online 16 April 2020
0016-2361/

as it is not linked to oil prices [3], but actions are necessary to block emissions now, as a short-term strategy.

The EPA estimates that most of the emissions of carbon dioxide derive from combustion to produce energy (fuel, electricity, etc.); 21% of the total global greenhouse emissions account for the industrial sector [4]. Green energy sources (even though intermittent) are available (solar, wind, marine) while alternative carbon feedstock to produce chemicals lack.

In the period 2017–2020, 9839 scientific documents have been published regarding carbon dioxide capture and storage (CCS) (research made the 27/03/2020 in the *Topic* field of Web of Science Core Collection with the keywords *"(carbon dioxide capture) OR (Carbon capture and storage)"*). CCS technologies rely on the absorption and mineralization of carbon dioxide over solids or liquids [5]. However, high process costs [6] and technical issues, such as corrosion [7], limit the expansion of CCS at larger scale. Hansan et al. estimated that the sequestration of CO_2 whose concentration in a gas stream is higher than 10% costs from 30 $/t to 70 $/t of CO_2, depending on the flow rate and the composition of the exhausted [8]. Moreover, a survey conducted in Germany in 2016 revealed that population rejects the CSS (sub-sea) compared to alternative remedies such as afforestation because of a general skepticism [9].

According to the IEA [10], CCS, CCSU, reduction of upstream oil consumption, nuclear energy and energy switching could decrease the CO_2 emissions up to 28%. The impact on the total emissions of the production of fuels or chemicals from CO_2 could represent a reduction between 5% to 20% of them [11–13].

Converting CO_2 into chemicals or fuel is another profitable strategy that enables the reuse of carbon instead landfilling it. Methanol is a bulk chemical and a reagent for the production of various added value chemicals, like formaldehyde [14,15], olefins [16,17], biodiesel [18–20], aromatics [21,22]. Methanol is an energy vector as well [23]. The annual world methanol production is increasing, in 2016 it was 80 Mt and it is expected to reach 100 Mt in 2020 [24]. The main reactions during the methanol synthesis are:

$$CO_{(g)} + 2H_{2(g)} \rightleftharpoons CH_3OH_{(g)} \quad (\Delta H^0_{533K} = -136.9 \text{kJ mol}^{-1}) \tag{1}$$

$$CO_{2(g)} + 3H_{2(g)} \rightleftharpoons CH_3OH_{(g)} + H_2O_{(g)} \quad (\Delta H^0_{533K} = -97.36 \text{kJ mol}^{-1}) \tag{2}$$

$$CO_{2(g)} + H_{2(g)} \rightleftharpoons CO_{(g)} + H_2O_{(g)} \quad (\Delta H^0_{533K} = +46.4 \text{kJ mol}^{-1}) \tag{3}$$

Methanol is produced by reaction (1) and (2), while reverse Water Gas Reaction (rWGS, reaction (3)) consumes part of the hydrogen producing H_2O and CO. Methanol synthesis reactions are exothermic and catalyzed by copper and zinc (CZA catalyst), while rWGS is an endothermic reaction. The atomic molar ratio of a CZA ($Cu/ZnO/Al_2O_3$) commercial catalyst is 60/30/10 with 1% to 3% by weight of MgO. Cu and Zn oxide, with alumina as structural promoter, catalyze the hydrogenation of CO [25]. The catalyst activity depends on the copper exposed area [26]. Assuming a regular distribution of copper, zinc and dopants, the higher the surface area the greater the activity of the catalyst is [27]. MgO increases the catalyst lifetime, stabilizing the CZA structure and avoiding decreasing of the exposed copper area due to thermal sintering [28]. However, MgO inhibits methanol formation [28,29]. In methanol synthesis reactions, the moles of products are lower than the moles of reactants (Eqs. (1) and (2)), therefore high pressures thermodynamically favor methanol formation. Industrial reactors typically operate at a pressure from 5 MPa to 10 MPa [30,31] with average CO conversion per pass of 25% and a selectivity towards methanol over 99% [32]. Moderate temperatures (473 K to 573 K) avoid thermodynamic limitations due to the reaction exothermicity. CO_2 is co-fed in low percentages (from 0.5% to 5%) to increase methanol productivity [33]. Data are available on carbon dioxide conversion at medium pressure (over 5 MPa) while literature is lacking of data under 2.5 MPa. Working at lower pressures allows energy and cost savings, which leads to a greener and more remunerative processes. For example, a plant that produces methanol from water electrolysis and biomass gasification consumes about 10% of the energy in gas compression [34]. Another limitation is the large excess of hydrogen employed in the feed: Meshkini et al. employed a mixture of CO_2 and syngas with 87.8% of hydrogen [35]. This decreases the economic competitiveness of the process proposed and limits its scale up. They reported that Mn and Zr improve the methanol space time yield after 60 h of operation (500 g kg^{-1} h^{-1} and 520 g kg^{-1} h^{-1}, respectively compared to 490 g kg^{-1} h^{-1} for the undoped catalyst). As far as we know, no one tested the effect of calcium oxide on the catalyst activity of CZA at low pressure. The ideal feed has the lowest pressure and percentage of hydrogen possible (the stoichiometric amount). Here we test four different CZA catalysts in the conversion of syngas, a simulated biosyngas and a stream of CO_2 and H_2 into methanol. We study a commercial CZA by Alfa Aesar (CZA-C) and three catalysts prepared i) without the addition of Mg (CZA-S) and two doped with either ii) Ca (CZA-Ca) or iii) Sr (CZA-Sr). This paper is original because: we study the methanol synthesis with different gas composition but without an excess of hydrogen, aiming at developing a more economical process performing the reaction at low pressure and we test the activity of CZA-Ca and CZA-Sr, which was never reported in literature before. We also characterized a sample prepared with the same co-precipitation method employing Mg as promoter.

2. Experimental

2.1. Catalyst synthesis

CZA catalysts were synthesized with a co-precipitation method [36]. Distilled water dissolved metal nitrates precursors ($Cu(NO_3)_2$, $Zn(NO_3)_2$, $Al_2(NO_3)_3$, $Mg(NO_3)_2$, $Sr(NO_3)_2$, and $Ca(NO_3)_2$, purity 95%, Sigma Aldrich) with a total concentration of 1.0 mol K^{-1} and a metal molar ratio of 60-30-10-1, respectively for Cu, Zn, Al and X, where X is Ca, Mg or Sr. We selected this percentage to avoid excessive covering of the basic promoter and to have a comparable concentration comparable to the one employed in literature [29,35,37]. We added the metal solution to 200mL of distilled water in a jacket reactor. A syringe pump controlled the metal solution flow, set to 5mL min^{-1}. A thermocouple and a pHmeter monitored the operating condition. The simultaneous addition of a Na_2CO_3 solution (1.0 mol L^{-1}) maintained the pH to a value of 7 ± 0.2. A thermostatic bath set the temperature of the reactor to 343 K. After the metal solution addition, the mixture aged for 1 h at 343 K and pH = 7. A Buchner filtered the blue precipitate. It was washed with 150mL of deionized water and dried at 353 K for 15 h in an oven. A furnace calcined the powder at 573 K under static air for 3 h (ramp of 15 K min^{-1}). A sieve meshed the resulting catalyst in the range 106 mm to 136 mm to avoid mass transfer limitations in the reaction.

2.2. Characterization

We characterized all synthesized samples before testing them. A Micromeritics Tristar II apparatus (Tristar II 3020) measured the Brunauer-Emmett-Teller (BET) specific surface area from N_2 adsorption/desorption isotherms at 77 K [38]. Barret-Joyner-Halenda (BJH) method applied to the N_2 adsorption data evaluated porosity distribution [39]. We pre-treated the samples at 423 K for 4 h under a N_2 flow to remove adsorbed water and contaminants. A LEO1525 Field emission scanning electron microscope (SEM) imaged all the samples. A Bruker Quantax EDX instrument equipped on the SEM mapped elements' distribution on catalysts' surface. X-ray photoelectron spectra (XPS) were taken in an M-probe apparatus (Surface Science Instruments). The source was monochromatic Al Kα radiation (1486.6 eV). A Philips PW3020 diffractometer (XRD) collected samples' diffractograms from 10° to 65° with a step of 0.04° (step time of 10 s). Temperature

programmed reduction (TPR) analyses measured the reduction temperature of Cu to metal [40]. 50 mg of samples reacted with 40 mL min^{-1} of 5% of H_2 (in Ar) ramping the temperature from 298 K to 1173 K at 10 K min^{-1}. A thermoconductivity detector (TCD) measured H_2 uptake. A Mettler Toledo TGA/DSC 3+ characterized CZA-S before and after the synthesis and estimated the amount of carbon coke remained on the catalyst after the reaction. TGA measured weight variation of the sample under an air flux, ramping the temperature from 313 K to 973 K at 5 K min^{-1}.

2.3. Bench scale plant

We charged (1.00 ± 0.01) g of catalyst in a 6.35 mm diameter reactor (reactor length = 560mm). A blank test assured that its internal surface is inactive. Two pieces of quartz wool held the catalyst in place, in a fixed bed configuration. Prior to the test, 20 NmL min^{-1} of H_2 reduced the catalyst *in situ* at 573 K for 3 h. Then, four mass flow controllers flowed nitrogen (internal standard for chromatographic analyses), carbon monoxide, hydrogen and carbon dioxide into the reactor. A pressure controller back-regulated the pressure to a value of 2 MPa. An electrical furnace heated the reactor to the desired temperature. A K-type thermocouple measured the reaction temperature right above the catalytic bed. We profiled the isothermal zone of the reactor (Supporting information, Fig. S1). Reactants flow from the top to the bottom of the reactor with a GHSV of 4030 h^{-1}. Before the pressure controller, a cold trap (T = 265 ± 1 K) condenses the reaction products (methanol and water). A micro-GC (Agilent 3000A, carrier: He), equipped with a PlotQ and a MOLSIEVE columns, samples the exiting gases every 1 h. It calculates the flow of CO that exits the reactor ($F_{CO,out}$) using the flow and peak area of the internal standard (N_2, Eq. (4)) and, therefore, CO conversion (X_{CO}, (5)) [41]. The micro-GC also detects methanol that is not condensed.

$$F_{CO,out} = F_{N2,in} * \frac{Area_{CO}}{Area_{N2}} \quad (4)$$

$$X_{CO} = \frac{F_{CO,in} - F_{CO,out}}{F_{CO,in}} * 100 \quad (5)$$

$$S = \frac{F_{H_2,in} - F_{CO_2,in}}{F_{CO_2,in} + F_{CO,in}} \quad (6)$$

At the end of each test, a GC-FID Fision 8000, equipped with a Porapak column QS, determined the methanol concentration in the cold trap, using acetone (Sigma Aldrich, 99% purity) as internal standard. The oven temperature was 573 K, the carrier was He at a inlet pressure of 100 kPa. The attenuation and the range were 1 and 2 respectively. We tested CZA-C, -S, -Ca and -Sr catalysts with: a) syngas, with a H_2/CO molar ratio of 2, to simulate a stoichiometric amount of reactants produced by methane steam reforming [42,43], which is also the typical feed composition for Fischer-Tropsch reactors [44–46], b) syngas containing 5.6% of CO_2, which is similar to the composition obtained by steam-gasification of biomass-derived oil (carrier gas: N_2 and T = 1073 K) [47] and a H_2 concentration of 72%. In this feed, H_2 concentration was set to have a S value of 2.4 (Eq. (6)). S considers the extra amount of H_2 that CO_2 consumes in the rWGS [48]. A value $S = 2$ corresponds to the stoichiometric H_2 quantity. Nevertheless, in commercial processes a value higher that 2 is employed (2.2–2.4). Finally, catalysts were tested with a c) stoichiometric mixture of CO_2 and H_2 (1:3), to study the direct conversion of carbon dioxide into methanol (Table 1). The reactor operated between 513 K to 533 K as most of CZAs have a maximum conversion of CO_2 [29]. We set the pressure to 2 MPa because Saeidi et al. [49] reported from many catalysts for CO_2 conversion this operating pressure.

Table 1
Summary of the experiments for CZA-C, CZA-S, CZA-Ca and CZA-Sr.

Test	Temperature, K	Flow rate set, NmL min^{-1}			
		CO	H_2	CO_2	N_2
1	513	10.4	33.7	2.6	5.0
2	533	10.4	33.7	2.6	5.0
3	513	–	31.3	10.4	5.0
4	533	–	31.3	10.4	5.0
5	513	15.6	31.1	–	5.0
6	533	15.6	31.1	–	5.0

3. Results and discussion

During TGA analysis, CZA-S loses weight in the ranges 373 K to 473 K (Fig. 1, A), 523 K to 673 K (Fig. 1, B) and, 723 K to 873 K (Fig. 1, C), in accordance with the data reported by Gines et al. [50,51]. Firstly, crystallized water contained in hydroxycarbonates evaporates. The complete dehydroxylation occurs as the second peak and the decarbonation with the loss of strongly bonded CO_3^{2-} constitutes the third peak [51]. During sample preparation, at 573 K, hydroxycarbonates partially dehydroxylate and decompose [52,53], therefore oxides may form in this second step.

XRD analyses confirm this observation. For CZA-S, CZA-Ca and CZA-Mg, indeed, typical peaks of copper and zinc oxide are observed (Fig. 2). Moreover, in CZA-Ca peaks of crystalline $CaCO_3$ are also evidenced (Circular of the Bureau of Standards n. 539: standard X-ray diffraction powder patterns). CZA-Sr has a similar behavior, with the presence of $SrCO_3$. In CZA-Mg, $MgCO_3$ peaks are absent (Fig. 2), as also observed in [51], even though also its degradation temperature is higher than 573 K.

Mg^{2+} has a radius close to copper and the same charge [54] and therefore it substitutes copper in the lattice, without forming $MgCO_3$, which is not detected in XRD spectra. CZA-S and CZA-C have a similar structural morphology, *i.e.* agglomerated spherical particles randomly organized (Fig. 3a–d). Doping the catalyst with Ca and Sr induces the formation of well-organized rod-like structures constituted by smaller nanoparticles. Sr makes the rods cover the main structure (Fig. 3g and h). Baltes et al. obtained a similar conformation applying the same synthesis conditions [36]. These structures are similar to polycrystalline calcite needle-fiber, formed by random precipitation around nuclei in the presence of highly supersaturated solution [55]. These columnar structures are absent in CZA-Mg (Fig. 3i–j), whose morphology is similar to CZA-S. These differences are due to carbonates water solubility ($MgCO_3$, 1.4 × 10^{-1} g L^{-1}, $CaCO_3$, 1.4 × 10^{-2} g L^{-1}, and $SrCO_3$, 3.4 × 10^{-3} g L^{-1} [56,57]), that induces a different relative supersaturation (*RS*) of these salts in solution during the synthesis (*RS* = 0, 11 and 73 for $MgCO_3$, $CaCO_3$, $SrCO_3$, respectively). Indeed, during the precipitation step, alongside the formation and growth of hydroxycarbonates (the core of CZA), alkaline earth metal carbonates form and are stable at the synthesis conditions [58,50]. In our synthesis, the concentration of $MgCO_3$ was not in supersaturated conditions.

Hydroxycarbonates have a $pH_{p.z.c.}$ above 7 [59]. The pH during the synthesis is about 7, and hydroxycarbonates, positively charged, attract negative species as carbonates that interact preferably with the formed solid rather than dissolved cations in solution [60]. These particles attract the solute clusters (embryos) by Van der Waals forces [61]. The concentration of embryos in the proximity of the forming crystals depends on the supersaturation of the solution, the larger the *RS* the higher their concentration [61]. When *RS* is large a rapid coagulation happens, leading to the formation of nuclei greater than a critical size, above which there is the nucleation [61]. These superstructures based on chaotically assembled nanoparticles precipitate on the hydroxycarbonates. This phenomenon is defined as secondary nucleation and is responsible of the structures observed when doping with Ca and Sr. The difference between these two alkaline earth metals is related to the

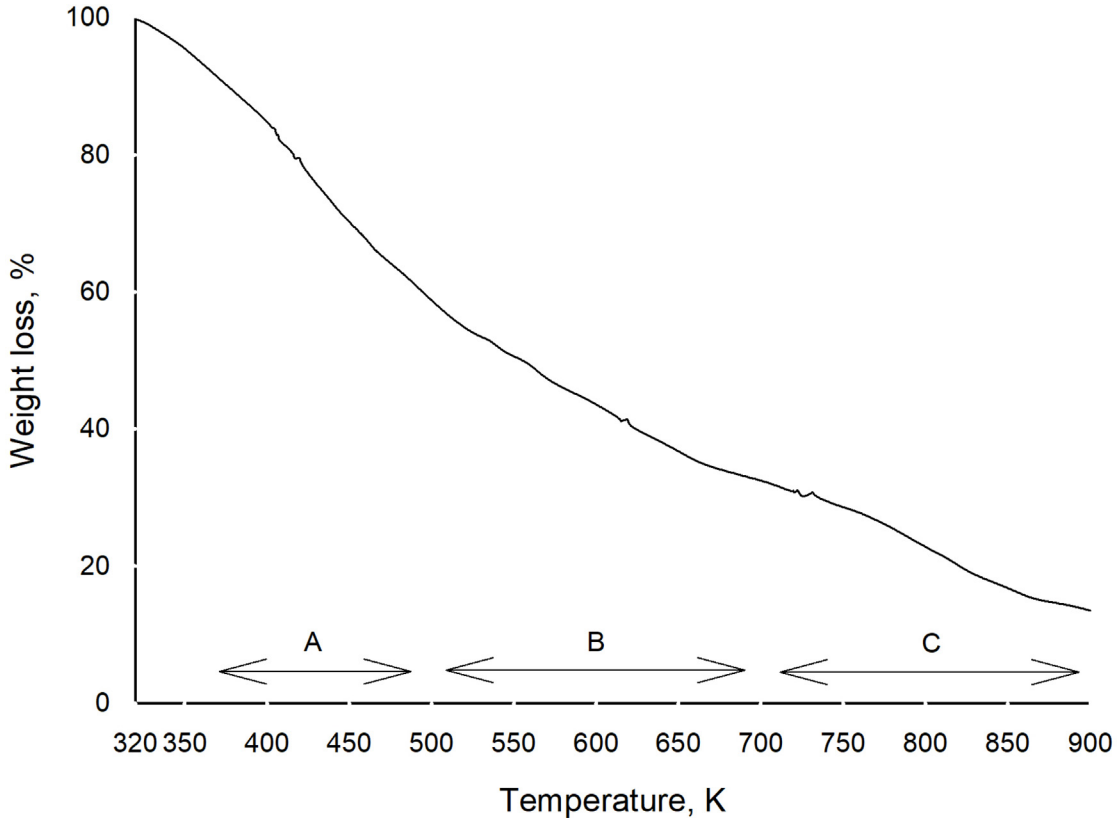

Fig. 1. Thermal Gravimetric Analysis of CZA-S.

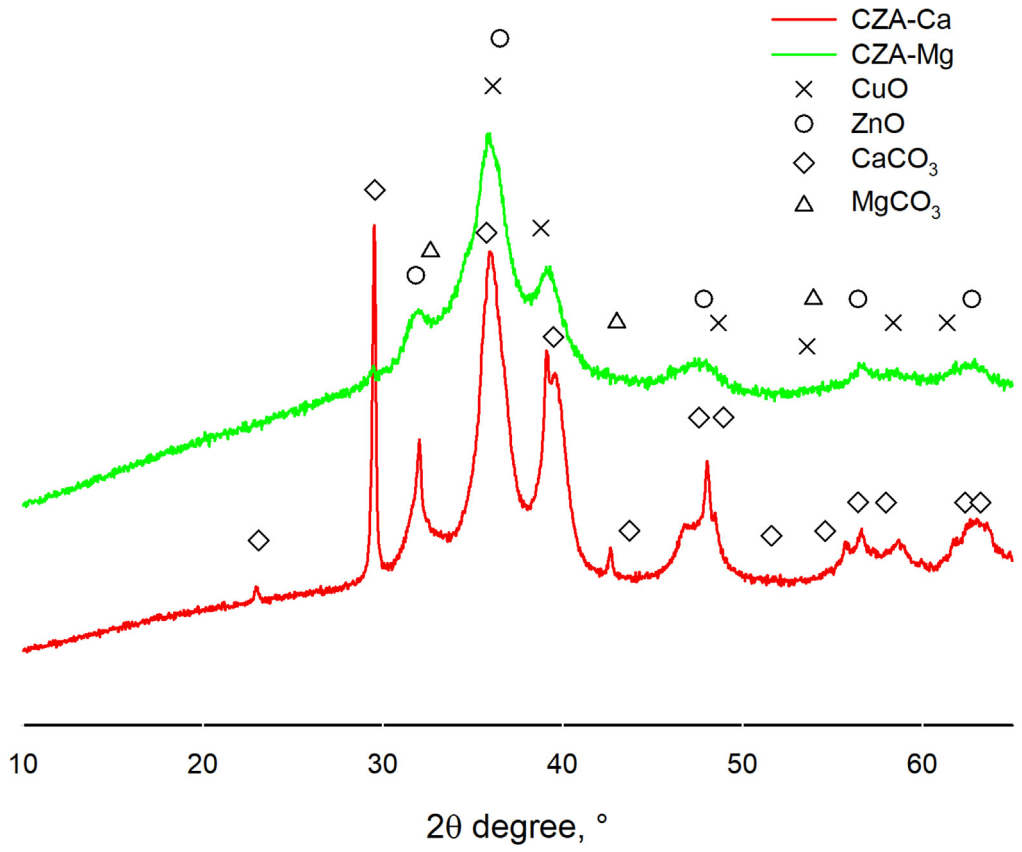

Fig. 2. XRD analyses.

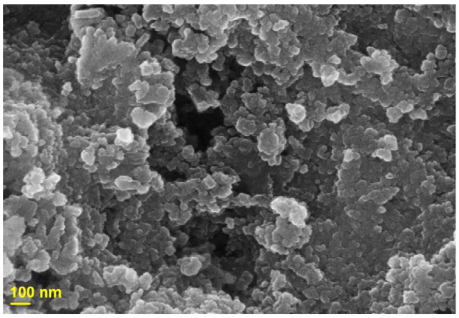

(a) CZA-C, magnification: 100K

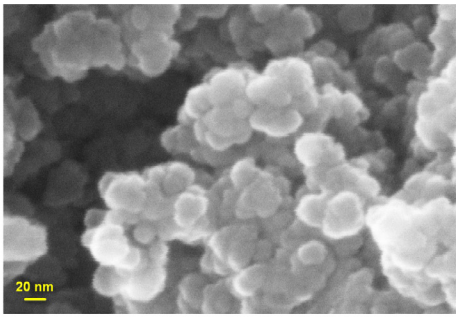

(b) CZA-C, magnification: 500K

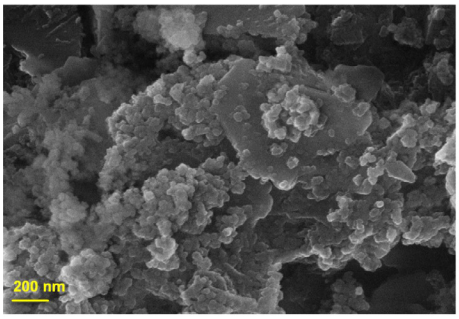

(c) CZA-S, magnification: 100K

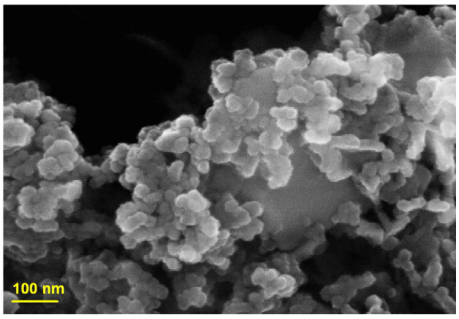

(d) CZA-S, magnification: 250K

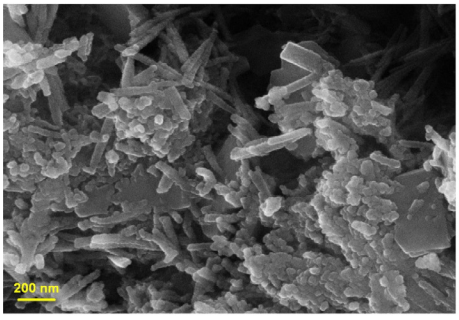

(e) CZA-Ca, magnification: 100K

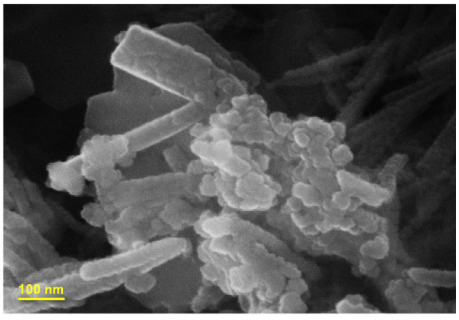

(f) CZA-Ca, magnification: 250K

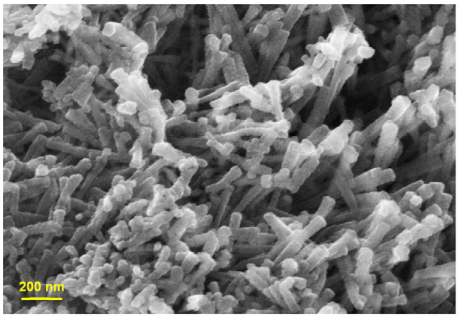

(g) CZA-Sr, magnification: 100K

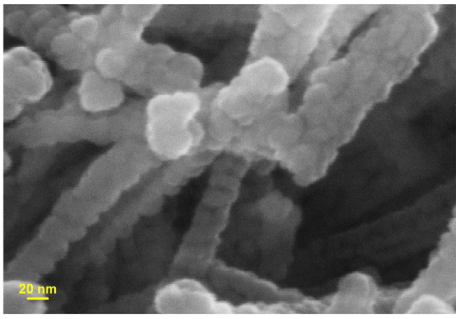

(h) CZA-Sr, magnification: 500K

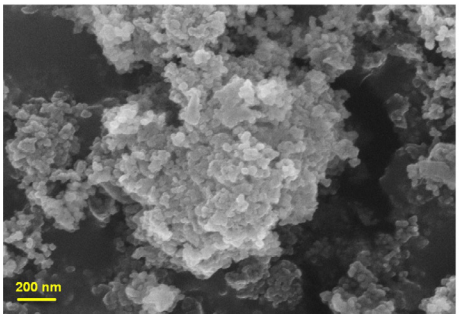

(i) CZA-Mg, magnification: 100K

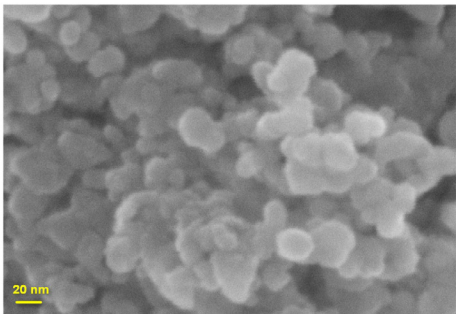

(j) CZA-Mg, magnification: 500K

(caption on next page)

Fig. 3. SEM images of commercial and synthesized CZA.

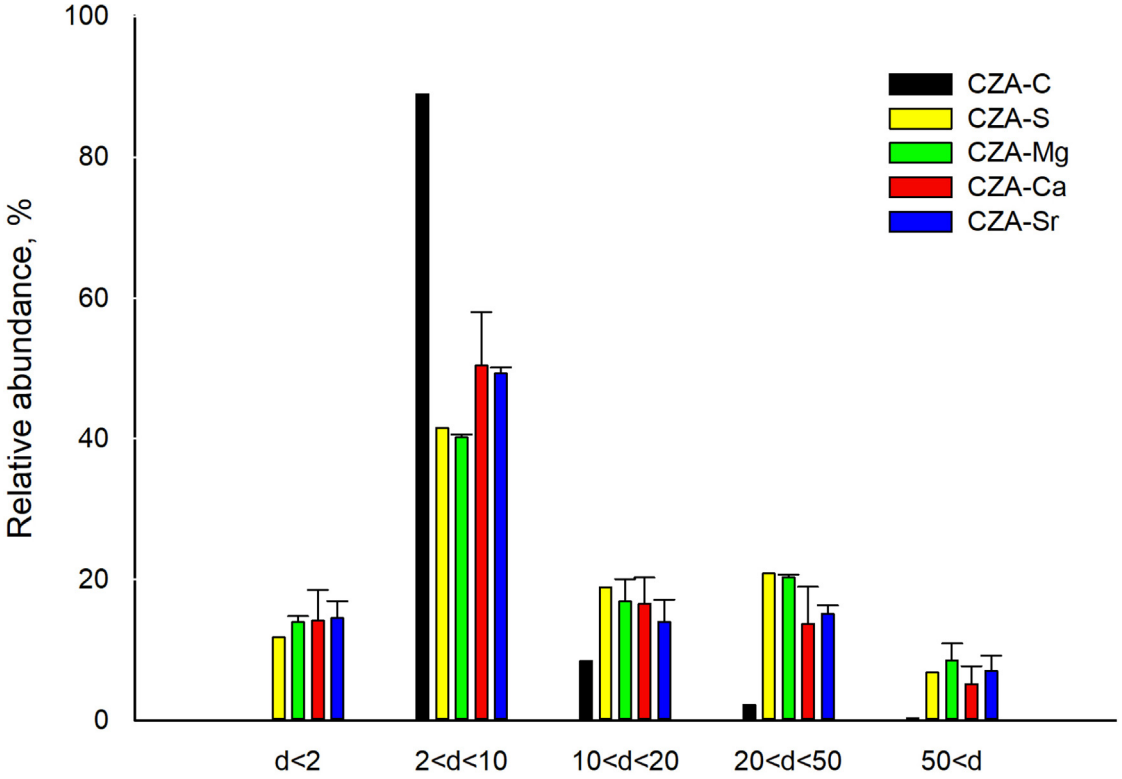

Fig. 4. Pore diameter distribution obtained from BJH model (adsorption branch of the isotherm).

different *RS* value, being in the case of Sr higher than Ca. In the case of doping with Mg, the solution is not supersaturated and these structures do not grow.

These structures affect the porosity distribution (Fig. 4) in the range of pores between 2 nm and 10 nm. In fact, doping with Ca and Sr, the amount of pores in this range is higher than in the case of both CZA-S and CZA-C. This difference is due to the porosity created between the building-blocks of the rod-like structures. The growth of these structures may also explain the lower specific surface area and pore volumes of these materials (Table 2) compared to commercial and undoped samples.

In fact, the secondary nucleation, responsible of these structures, may take place both onto the surface and in bigger pores, partially occluding them and provoking a decrease of both specific surface area and pore volume. Indeed, samples without rod-like structures possess similar specific surface area. Moreover, CZA-C does not present micropores, while all the other samples do. The majority of pores diameters' fall in the range 2 nm to 10 nm (above 40%), especially in the case of commercial sample (90% of the total). However, in CZA-Ca e CZA-Sr these pores are in a lower amount than in the other samples, and this might be justified considering the formation of rod-like structures as stated above.

All catalysts start to reduce in the range 473 K to 493 K, with a sharp peak from 539 K to 557 K, which corresponds to the transformation of CuO into Cu^0 (Fig. 5), in accordance with literature [62,63]. Therefore, the activation temperature chosen permitted to reduce copper. All samples present a minor and broad reduction peak between 873 K to 1043 K. It corresponds to the partial reduction of ZnO [64]. TPR confirms the presence of a sole copper species for CZA-S at 573 K, ascribable to the reduction of highly dispersed CuO [65]. The peak position of CZA-Mg is similar to that of CZA-S, with a broad peak between 593 K to 653 K. Ca and Sr doping shifts and broadens the reduction peak of CZA (inset of Fig. 5) because of the stronger interaction between the two lattice of CuO and ZnO [66].

SEM-EDX analysis shows a good distrubution of each metals for all catalyst samples (see Supporting information, Figs. S2–S4) and no traces of carbon (coke) were present on the spent catalysts. TGA diagrams report an increase of weight for CZA-S. This phenomenon is probably caused by copper oxidation. When CZA is discharged, the reactor is cold (T = 303 K) and not all the metallic copper is oxidized by

Table 2
BET area, pore volume and surface composition results (EDX and XPS) for all catalysts synthesized.

Catalyst	Morphology		Chemical composition						
	BET area m^2g^{-1}	Pore volume m^2g^{-1}	Al	Cu	Zn	O	Mg	Ca	Sr
			atomic %, XPS/ EDX (± 0.5)						
CZA-C	100 ± 1	0.19	40.2/ 7.8	12.8/ 21.2	8.8/ 9.6	38.2/ 60.4	–/ 1.5	–	–
CZA-S	94.9 ± 0.4	0.49	34.6/ 8.1	13.0/ 15.5	10.0/ 10.1	42.4/ 66.4	–	–	–
CZA-Ca	81.8 ± 0.4	0.28	38.6/ 8.3	11.6/ 17.7	7.0/ 13.8	42.8/ 60.0	–	0.0/ 0.2	–
CZA-Sr	71.8 ± 0.3	0.28	44.0/ 6.8	12.2/ 33.3	6.1/ 15.0	37.7/ 44.1	–	–	0.0/ 0.7
CZA-Mg	97.1 ± 0.3	0.59	32.8/ 1.1	3.8/ 29.4	5.1/ 8.5	33.3/ 61.0	25.0/0.1	–	–

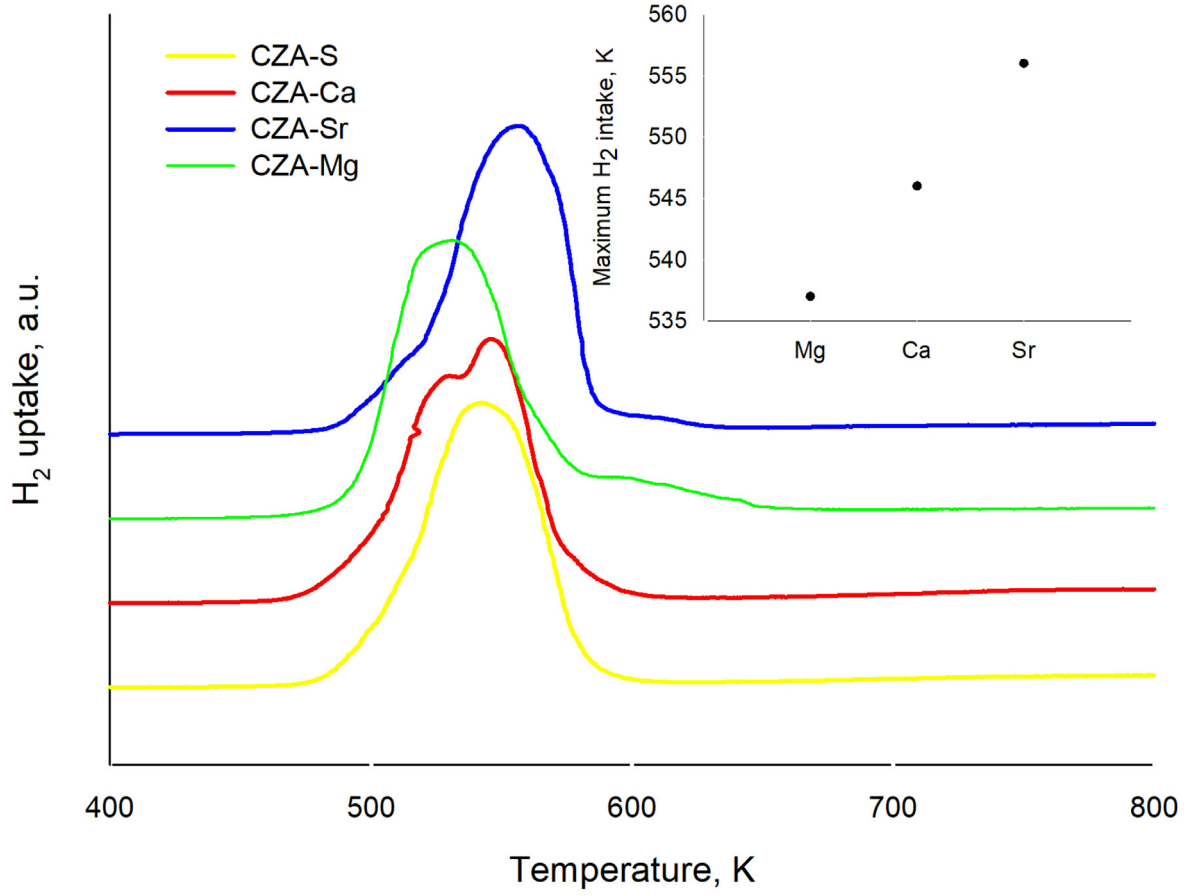

Fig. 5. Temperature programmed reduction of the synthesized catalysts.

atmospheric oxygen. The remaining Cu^0 reacts during the TGA analysis and CuO formation determines an increase in weight. This theory is confirmed also by the fact that the weight gain usually is 1.3 mg which corresponds to the quantity of oxygen necessary to oxidizes about 10% of the all metallic copper (see Supporting information, Fig. S5). XPS reports a surface enrichment of aluminum, as also reported in [67]. Its concentration reaches the maximum in the first layers of the particles (XPS measures from 38% to 40% atomic percentage of Al) and decreases after few micrometers depth (SEM-EDX measures from 7% to 8% atomic percentage of Al). This enrichment is due to the hydrolysis of the nitrate system [68].

All the catalytic tests have a mass balance for carbon and oxygen over 90%. With syngas (CO/H_2) as feed, the carbon conversion is higher at 533 K (Fig. 6b) due to kinetic reasons. We did not observe the typical volcano-shape curve for CO conversion because we operated the reactor at only two temperatures, near to the average maximum value (523 K, [29]) to have a comparison of the catalysts at similar thermodynamic and kinetic conditions. The activity of CZA-Ca is significantly higher (12% CO conversion (Table 3) respect to 9% for CZA-S) already at 513 K and increases at 533 K producing more than the double amount of products respect to CZA-C and maintaining a similar methanol content in the condensed fraction (Fig. 7)). CZA-S has an overall productivity similar to CZA-Ca at 513 K but with a methanol concentration lower than 20% (Fig. 7) by weight. The presence of Ca and Mg (the latter contained in CZA-C) limits the rWGS, the main source of water, at 513 K and 533 K where its endothermicity favors water formation. At 513 K, CZA-Ca has a stationary CO conversion value of about 5.6% while CZA-S the one with the lower conversion (3.9%). At 533 K the same trend was observed (11.5% versus 9.1%, Table 3). This is confirmed by the productivities of both methanol and water (Fig. 7). With syngas, Ca improves methanol formation by 3 times while the water content remains low (about 30% by weight). CZA-S has the worst performances as methanol productivity and as water content. The pore size dimension and distribution does not have an effect on CO or CO_2 conversion and methanol productivity (See Fig. 8).

With CO_2/H_2 as feeding mixture, temperature has a negligible influence on CO_2 conversion with CZA-C. The same trend is obtained observing the productivities (Fig. 7). Due to the large presence of CO_2 and H_2, high temperature favors the reverse Water Gas Shift reaction (rWGS) increasing the water and CO productivity while methanol concentration in the liquid product decreases. For this reason, with this feed are obtained the highest values of water concentration. CZA-C is the more stable varying the temperature while both CZA-Ca and CZA-S show an increase in CO_2 conversion of 2 or 3 times. Also in this case an increase of temperature cause a decreasing of methanol concentration. CZA-Sr resulted the least active.

Using as feed the mixture of CO and CO_2 at 513 K, the more active catalyst is CZA-S followed by CZA-C (about 20% less, Table 3) and CZA-Ca with the lowest productivity For CZA-C at 533 K the productivity increases despite the CO conversion decreases. This could be explained by an increase of selectivity of CO_2 to methanol instead of to CO and water (rWGS). This effect is emphasized with CZA-S where no promoters are present. Liu et al. obtained the same result with a Cu based catalyst supported on titania and modified with 1% of MgO [69]. They explained this behavior considering kinetics and thermodynamics. The presence of $MgCO_3$ results in a stronger CO_2 adsorption that improves its activity in terms of conversion. $CaCO_3$ is a stronger base than $MgCO_3$, and indeed the CO_2 conversion increases (Fig. 6)). CZA-C and CZA-Ca maintain similar productivity in terms of liquid quantity and composition at the two temperature tested. However, for CZA-S, increasing the temperature, the methanol formation is halved. CZA-Ca has the lowest productivities at both temperatures among the active

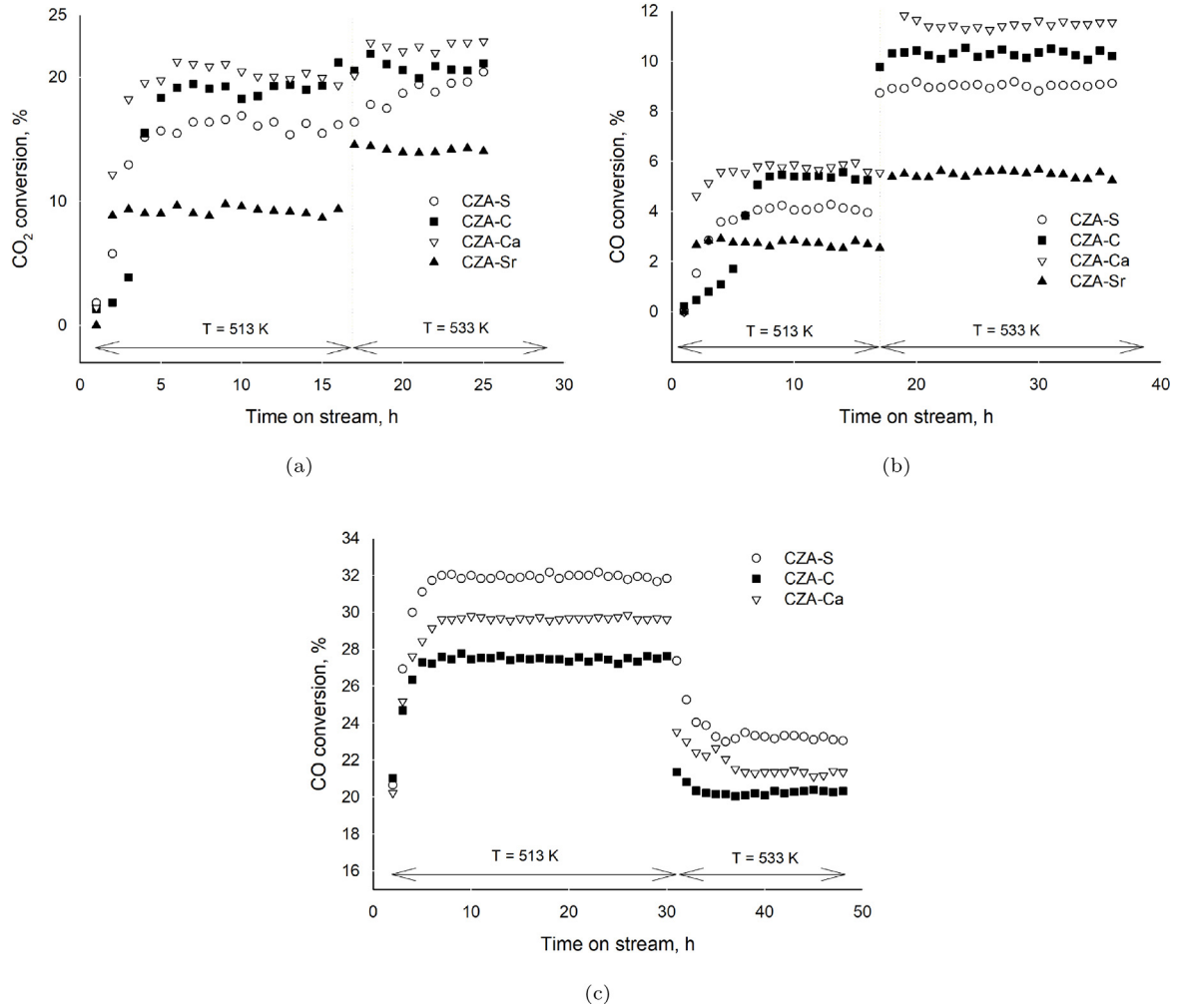

Fig. 6. Conversion of CO_2 or CO for all catalysts with different feed compositions: CO_2 and H_2 (a), CO and H_2 (b) and CO_2, CO and H_2, (c). CZA-Sr resulted inactive with this latter stream.

catalysts, while CZA-Sr resulted inactive with this feed (CO conversion lower than 3% for both the temperatures tested). Phongamwong et al. [70] derived an equation to calculate methanol selectivity and to assess the quantity of CO_2 converted to methanol (Table 4). Except for CZA-Sr, which resulted inactive for the neglible amount of methanol condensed in the cold trap, all the catalysts increases CO_2 conversion into CH_3OH at 533 K. Therefore, higher temperature activates carbon dioxide for this reaction. CZA-S and CZA-Ca resulted superior, probably because of the larger pore volume available compared to CZA-C (Table 2). The stationary state conversion of carbon at 513 K and 533 K demonstrated that the best promoter is not the most basic (Fig. 6), indeed Ca resulted the most active sample for all the feedstock tested. A deeper investigation on the diverse carbonate stability at different temperature and CO_2 partial pressures and on the dimension of the crystallites may correlate these findings.

Our materials are better than commercial one, and among homemade catalysts CZA-Ca shows with CO/H_2 and CO_2/H_2 the best performance in terms of methanol yield. These results may be justified considering porosity results. Despite many factors influence methanol yield, as stated by Li et al. [71], specific surface area has a great effect in this process, but pore volume and mesoporosity centered between 2 nm to 10 nm are both more pivotal. CZA-C posseses the highest specific surface area but also the lowest pore volume (Table 2), even if pores are centered in the optimal range, whilst CZA-Ca is characterized by a lower specific surface area and amount of pores centered in small mesopores but a larger pore volume (Table 2). For the other samples the results can be justified considering the combination between pore volume and mesoporosity. These data show that porosity and its distribution are important for catalytic activity in this process.

Table 3
Carbon conversion and sample standard deviation (in parenthesis) for all the tests.

Temperature, K	513			533		
Feed	H_2/CO	$H_2/CO/CO_2$	H_2/CO_2	H_2/CO	$H_2/CO/CO_2$	H_2/CO_2
CZA-S	4.0(0.2)	31.9(0.4)	16.0(0.5)	9.0(0.1)	23.4(0.2)	19.4(0.4)
CZA-C	5.4(0.1)	27.5(0.2)	19.0(1.0)	10.3(0.1)	20.3(0.3)	20.8(0.5)
CZA-Ca	5.7(0.1)	29.6(0.4)	20.3(0.8)	11.5(0.1)	21.8(0.4)	22.5(0.4)
CZA-Sr	2.7(0.1)	3.2(0.1)	9.2(0.3)	5.5(0.1)	3.0(0.1)	14.2(0.2)

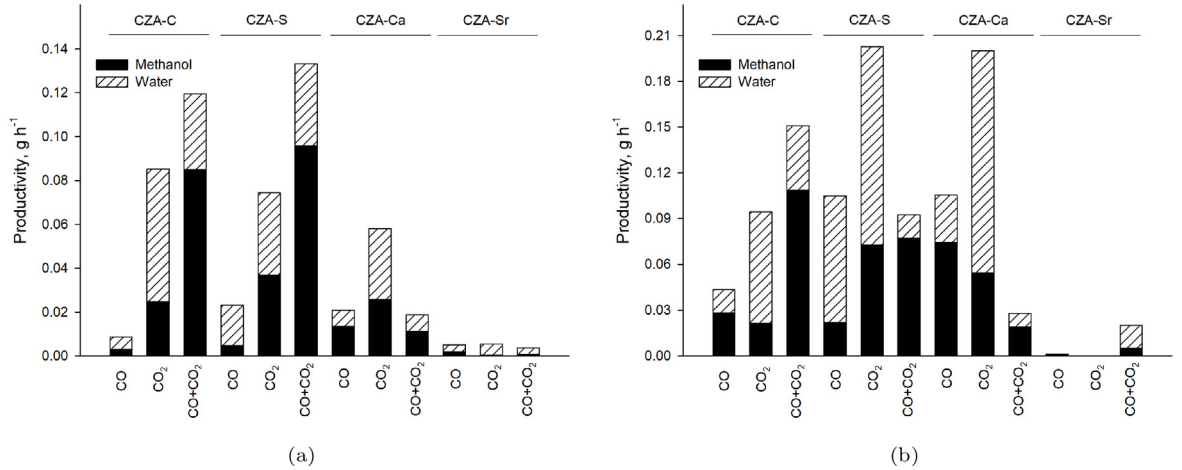

Fig. 7. Methanol and water productivity (divided by the total test time) at 513 K (a) and 533 K (b).

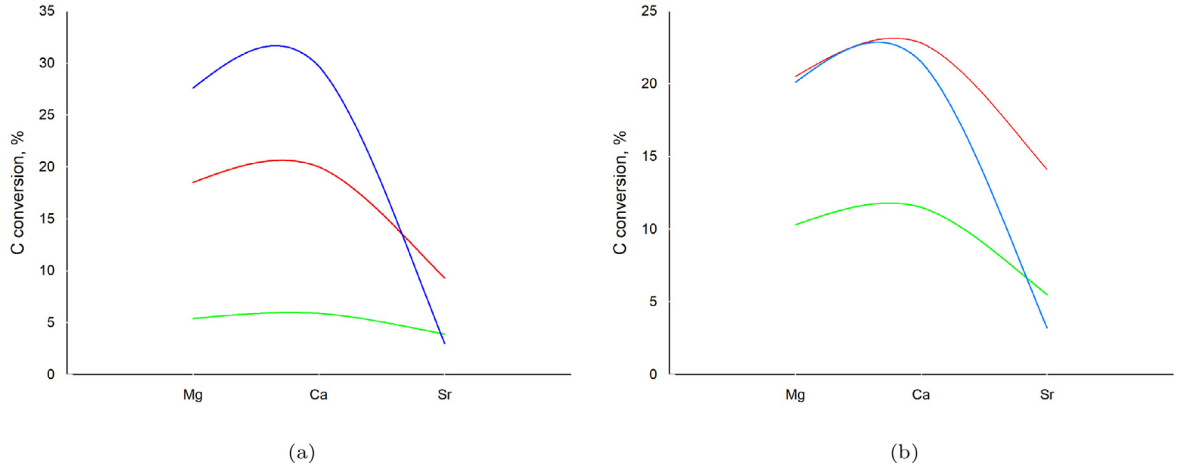

Fig. 8. Catalysts maximum carbon conversion at 513 K (a) and 533 K (b) versus basic promoter.

Table 4
Methanol selectivities and fraction of CO_2 converted into CH_3OH for the tests with CO_2 and syngas co-fed [70]. Uncertainties are reported in parenthesis with a confidence interval of 95%.

	CH_3OH selectivity, %		CO_2 to CH_3OH, %	
Temperature, K	513	533	513	533
CZA-C	0.2(0.0)	0.1(0.0)	3.8(0.1)	5.7(0.1)
CZA-S	0.4(0.0)	0.5(0.0)	4.3(0.3)	7.3(0.2)
CZA-Ca	0.2(0.0)	0.3 (0.0)	4.2(0.2)	6.5(0.2)
CZA-Sr	0.0(–)	0.0(–)	0.0(–)	0.0(–)

4. Conclusions

Methanol can be produced from biosyngas and streams of CO_2. However, at present, the industrialisation of this process is limited by economic constrains [72]. We doped a typical copper-zinc-alumina catalyst with 1% alkali earth metals to confer the final material basicity. These catalysts synthesize methanol at 2.0 MPa, with co-production of water. Sr resulted inactive towards CO_2 conversion into methanol. With syngas and CO_2/H_2 as feed, CZA-Ca resulted the best catalyst, with a CO conversion of 20% and 6% at 513 K and 24% and 12% at 533 K, respectively. The undoped catalyst possesses the highest CH_3OH selectivity and conversion of CO_2 into methanol, but literature reports low lifetime for these kind of materials. Metal doping tailor catalysts' morphology. Ca and Sr induce the formation of columnar structures. The catalysts were tested for 48 h at constant temperature, therefore little information is available on their stability over time, i.e. sintering, poisoning, etc. The synthesis of mixed oxide doped CZA and the effect of different dopants concentration will be the object of future works.

Declaration of Competing Interest

The authors declare that they have no known competing financial interests or personal relationships that could have appeared to influence the work reported in this paper.

CRediT authorship contribution statement

D. Previtali: Conceptualization, Methodology, Validation, Investigation, Writing - original draft. **M. Longhi:** Investigation, Data curation, Writing - original draft. **F. Galli:** Conceptualization, Methodology, Validation, Investigation, Writing - original draft, Visualization, Supervision. **A. Di Michele:** Investigation, Writing - review & editing. **F. Manenti:** Resources, Writing - review & editing. **M. Signoretto:** Data curation, Writing - review & editing. **F. Menegazzo:** Investigation, Writing - review & editing. **C. Pirola:** Writing - review & editing.

Appendix A. Supplementary data

Supplementary data associated with this article can be found, in the online version, at https://doi.org/10.1016/j.fuel.2020.117804.

References

[1] Schellnhuber HJ, Rahmstorf S, Winkelmann R. Why the right climate target was agreed in Paris. Nat Clim Change 2016;6(7):649–53. https://doi.org/10.1038/nclimate3013.

[2] Al-falahi MD, Jayasinghe S, Enshaei H. A review on recent size optimization methodologies for standalone solar and wind hybrid renewable energy system. Energy Convers Manage 2017;143:252–74. https://doi.org/10.1016/j.enconman.2017.04.019.

[3] Partridge I. Cost comparisons for wind and thermal power generation. Energy Policy 2018;112:272–9. https://doi.org/10.1016/j.enpol.2017.10.006.

[4] Global greenhouse gas emissions data. 2020.https://www.epa.gov/ghgemissions/global-greenhouse-gas-emissions-data.

[5] Rahman FA, Aziz MMA, Saidur R, Bakar WAWA, Hainin M, Putrajaya R, et al. Pollution to solution: capture and sequestration of carbon dioxide (CO_2) and its utilization as a renewable energy source for a sustainable future. Renew Sustain Energy Rev 2017;71:112–26. https://doi.org/10.1016/j.rser.2017.01.011.

[6] Gaede J, Meadowcroft J. Carbon capture and storage demonstration and low-carbon energy transitions: explaining limited progress. In: de Graaf Thijs V, KSB, Arunabha G, Florian K, TKM, editors. The Palgrave Handbook of the International Political Economy of Energy. London: Palgrave Macmillan UK. p. 319–340, ISBN 978-1-137-55631-8; 2016.https://doi.org/10.1057/978-1-137-55631-8_13.

[7] Barker R, Hua Y, Neville A. Internal corrosion of carbon steel pipelines for dense-phase co2 transport in carbon capture and storage (CCS) – a review. Int Mater Rev 2017;62(1):1–31. https://doi.org/10.1080/09506608.2016.1176306.

[8] Hasan MMF, Baliban RC, Elia JA, Floudas CA. Modeling simulation, and optimization of postcombustion CO_2 capture for variable feed concentration and flow rate. 1. Chemical absorption and membrane processes. Ind Eng Chem Res 2012;51(48):15642–64. https://doi.org/10.1021/ie301571d.

[9] Braun C, Merk C, Pönitzsch G, Rehdanz K, Schmidt U. Public perception of climate engineering and carbon capture and storage in germany: survey evidence. Clim Policy 2018;18(4):471–84. https://doi.org/10.1080/14693062.2017.1304888.

[10] World energy outlook 2018. 2018.https://www.iea.org/reports/world-energy-outlook-2018.

[11] Centi G, Perathoner S. Opportunities and prospects in the chemical recycling of carbon dioxide to fuels. Catal Today 2009;148(3):191–205. https://doi.org/10.1016/j.cattod.2009.07.075.

[12] Aresta M, Nocito F. Large scale utilization of carbon dioxide: From its reaction with energy rich chemicals to (co)-processing with water to afford energy rich products. opportunities and barriers. In: Aresta M, Karimi I, Kawi S, editors. An economy based on carbon dioxide and water. Cham: Springer International Publishing; 2019, p. 1–33.https://doi.org/10.1007/978-3-030-15868-2_1.

[13] Tapia JFD, Lee JY, Ooi RE, Foo DC, Tan RR. A review of optimization and decision-making models for the planning of CO2 capture, utilization and storage (CCUS) systems. Sustain Prod Consumpt 2018;13:1–15. https://doi.org/10.1016/j.spc.2017.10.001.

[14] Kropp T, Paier J, Sauer J. Oxidative dehydrogenation of methanol at ceria-supported vanadia oligomers. J Catal 2017;352:382–7. https://doi.org/10.1016/j.jcat.2017.06.011.

[15] Gribovskii A, Ovchinnikova E, Vernikovskaya N, Andreev D, Chumachenko V, Makarshin L. Microchannel reactor for intensifying oxidation of methanol to formaldehyde over Fe-Mo catalyst. Chem Eng J 2017;308:135–41. https://doi.org/10.1016/j.cej.2016.09.058.

[16] Losch P, Pinar AB, Willinger MG, Soukup K, Chavan S, Vincent B, et al. H-ZSM-5 zeolite model crystals: structure-diffusion-activity relationship in methanol-to-olefins catalysis. J Catal 2017;345:11–23. https://doi.org/10.1016/j.jcat.2016.11.005.

[17] Wang X, Li R, ul Hasnain Bakhtiar S, Yuan F, Li Z, Zhu Y. Excellent catalytic performance for methanol to olefins over SAPO-34 synthesized by controlling hydrothermal temperature. Catal Commun 2018;108:64–67.https://doi.org/10.1016/j.catcom.2018.01.033.

[18] Pirola C, Manenti F, Galli F, Bianchi CL, Boffito DC, Corbetta M. Heterogeneously catalyzed free fatty acids esterification in (monophasic liquid)/solid packed bed reactors (PBR). Chem Eng Trans 2014;37:553–8. https://doi.org/10.3303/CET1437093.

[19] Pirola C, Galli F, Bianchi CL, Boffito DC, Comazzi A, Manenti F. Vegetable oil deacidification by methanol heterogeneously catalyzed esterification in (monophasic liquid)/solid batch and continuous reactors. Energy Fuels 2014;28(8):5236–40. https://doi.org/10.1021/ef501397h.

[20] Boffito DC, Galli F, Martinez PR, Pirola C, Bianchi C, Patience GS. Transesterification of triglycerides in a new ultrasonic- assisted mixing device. Chem Eng Trans 2014;43:427–32. https://doi.org/10.3303/CET1543072.

[21] Niu X, Gao J, Wang K, Miao Q, Dong M, Wang G, et al. Influence of crystal size on the catalytic performance of H-ZSM-5 and zn/H-ZSM-5 in the conversion of methanol to aromatics. Fuel Process Technol 2017;157:99–107. https://doi.org/10.1016/j.fuproc.2016.12.006.

[22] Yang L, Liu Z, Liu Z, Peng W, Liu Y, Liu C. Correlation between H-ZSM-5 crystal size and catalytic performance in the methanol-to-aromatics reaction. Chin J Catal 2017;38(4):683–90. https://doi.org/10.1016/S1872-2067(17)62791-8.

[23] Iaquaniello G, Centi G, Salladini A, Palo E. Methanol economy: environment, demand, and marketing with a focus on the waste-to-methanol process. In: Basile A, Dalena F, editors. Methanol. Elsevier. ISBN 978-0-444-63903-5; 2018, p. 595–612. https://doi.org/10.1016/B978-0-444-63903-5.00022-4.

[24] Alvarado M. The changing face of the global methanol industry. IHS Chem Bull 2016;3(6083):10–1.

[25] Behrens M, Studt F, Kasatkin I, Kühl S, Hävecker M, Abild-Pedersen F, et al. The active site of methanol synthesis over Cu/ZnO/Al2O3 industrial catalysts. Science 2012;336(6083):893–7. https://doi.org/10.1126/science.1219831.

[26] Robinson W, Mol J. Copper surface area and activity in CO/H2 of Cu/ZnO/Al2O3 methanol synthesis catalysts. Appl Catal 1990;60(1):73–86. https://doi.org/10.1016/S0166-9834(00)82173-9.

[27] Azizi Z, Rezaeimanesh M, Tohidian T, Rahimpour MR. Dimethyl ether: a review of technologies and production challenges. Chem Eng Process 2014;82:150–72. https://doi.org/10.1016/j.cep.2014.06.007.

[28] Doesburg E, Höppener R, de Koning B, Xiaoding X, Scholten J. Preparation and characterization of copper/zinc oxide/alumina catalysts for methanol synthesis. In: Delmon B, Grange P, Jacobs P, Poncelet G, editors. Preparation of Catalysts IV; vol. 31 of Studies in Surface Science and Catalysis. Elsevier; 1987, p. 767–783.https://doi.org/10.1016/S0167-2991(08)65452-X.

[29] Fitzpatrick T, Hicks T. Catalysts with higher and more stable activity enable cost saving and boost output in methanol production. Catalysis 2010;15:47–53. URL: https://www.digita0lrefining.com/data/digital_magazines/file/1717768075.pdf.

[30] Lunkenbein T, Girgsdies F, Kandemir T, Thomas N, Behrens M, Schlögl R, et al. Bridging the time gap: a copper/zinc oxide/aluminum oxide catalyst for methanol synthesis studied under industrially relevant conditions and time scales. Angew Chem Int Ed 2016;55(41):12708–12. https://doi.org/10.1002/anie.201603368.

[31] English A, Rovner J, Brown J, Davies Sa. Methanol. In: Kirk-Othmer encyclopedia of chemical technology; chap. 16. American Cancer Society. ISBN 9780471238966; 2005, p. 299–316.https://doi.org/10.1002/0471238961.1305200805140712.a01.pub2.

[32] Yang L, Ge X. Chapter three – biogas and syngas upgrading. vol. 1 of Advances in Bioenergy. Elsevier; 2016, pp. 125–188.https://doi.org/10.1016/bs.aibe.2016.09.003.

[33] Ertl G, Knözinger H, Weitkamp J. Handbook of heterogeneous catalysis. Wiley; 2008.https://doi.org/10.1002/9783527619474.

[34] Clausen LR, Houbak N, Elmegaard B. Technoeconomic analysis of a methanol plant based on gasification of biomass and electrolysis of water. Energy 2010;35(5):2338–47. https://doi.org/10.1016/j.energy.2010.02.034.

[35] Meshkini F, Taghizadeh M, Bahmani M. Investigating the effect of metal oxide additives on the properties of Cu/ZnO/Al2O3 catalysts in methanol synthesis from syngas using factorial experimental design. Fuel 2010;89(1):170–5. https://doi.org/10.1016/j.fuel.2009.07.007.

[36] Baltes C, Vukojevic S, Schuth F. Correlations between synthesis, precursor, and catalyst structure and activity of a large set of CuO/ZnO/Al2O3 catalysts for methanol synthesis. J Catal 2008;258(2):334–44. https://doi.org/10.1016/j.jcat.2008.07.004.

[37] Wang Y, Kattel S, Gao W, Li K, Liu P, Chen JG, et al. Exploring the ternary interactions in Cu-ZnO-ZrO_2 catalysts for efficient co2 hydrogenation to methanol. Nat Commun 2019;10:1–10. https://doi.org/10.1038/s41467-019-09072-6.

[38] Brunauer S, Emmett PH, Teller E. Adsorption of gases in multimolecular layers. J Am Chem Soc 1938;60(2):309–19. https://doi.org/10.1021/ja01269a023.

[39] Barrett EP, Joyner LG, Halenda PP. The determination of pore volume and area distributions in porous substances. i. Computations from nitrogen isotherms. J Am Chem Soc 1951;73(1):373–80. https://doi.org/10.1021/ja01145a126.

[40] Pirola C, Galli F, Patience GS. Experimental methods in chemical engineering: temperature programmed reduction–TPR. Can J Chem Eng 2018;96(11):2317–20. https://doi.org/10.1002/cjce.23317.

[41] Skoog DA, West DM, Holler FJ, Crouch SR. Fundamentals of analytical chemistry. Nelson Education; 2013.

[42] Lutz AE, Bradshaw RW, Keller JO, Witmer DE. Thermodynamic analysis of hydrogen production by steam reforming. Int J Hydrogen Energy 2003;28(2):159–67. https://doi.org/10.1016/S0360-3199(02)00053-8.

[43] Wei J, Iglesia E. Isotopic and kinetic assessment of the mechanism of reactions of CH4 with CO2 or H2O to form synthesis gas and carbon on nickel catalysts. J Catal 2004;224(2):370–83. https://doi.org/10.1016/j.jcat.2004.02.032.

[44] Comazzi A, Pirola C, Bianchi CL, Galli F, Longhi M, Manenti F. High-loaded fe-supported catalyst for the thermochemical BtL-FT process: experimental results and modelling. Can J Chem Eng 2016;94(4):696–702. https://doi.org/10.1002/cjce.22357.

[45] Comazzi A, Pirola C, Michele AD, Compagnoni M, Galli F, Rossetti I, et al. Flame spray pyrolysis as fine preparation technique for stable co and co/ru based catalysts for FT process. Appl Catal A: General 2016;520:92–8. https://doi.org/10.1016/j.apcata.2016.04.010.

[46] Louyot P, Neagoe C, Galli F, Pirola C, Patience GS, Boffito DC. Ultrasound-assisted impregnation for high temperature Fischer-Tropsch catalysts. Ultrason Sonochem 2018;48:523–31. https://doi.org/10.1016/j.ultsonch.2018.06.017.

[47] Panigrahi S, Dalai AK, Chaudhari ST, Bakhshi NN. Synthesis gas production from steam gasification of biomass-derived oil. Energy Fuels 2003;17(3):637–42. https://doi.org/10.1021/ef020073z.

[48] Bozzano G, Manenti F. Efficient methanol synthesis: perspectives, technologies and optimization strategies. Prog Energy Combust Sci 2016;56:71–105. https://doi.org/10.1016/j.pecs.2016.06.001.

[49] Saeidi S, Amin NAS, Rahimpour MR. Hydrogenation of CO_2 to value-added products–a review and potential future developments. J CO_2 Util 2014;5:66–81. https://doi.org/10.1016/j.jcou.2013.12.005.

[50] Ginés MJL, Apesteguía CR. Thermal decomposition of cu-based hydroxycarbonate catalytic precursors for the low-temperature co-shift reaction. J Therm Anal 1997;50(5):745–56. https://doi.org/10.1007/BF01979204.

[51] Zhang F, Zhang Y, Yuan L, Gasem KA, Chen J, Chiang F, et al. Synthesis of Cu/Zn/Al/Mg catalysts on methanol production by different precipitation methods. J Mol Catal 2017;441:190–8. https://doi.org/10.1016/j.mcat.2017.08.015.

[52] Frost R, Ding Z, Kloprogge J, Martens W. Thermal stability of azurite and malachite

in relation to the formation of mediaeval glass and glazes. Thermochim Acta 2002;390(1):133–44. https://doi.org/10.1016/S0040-6031(02)00127-2.
[53] Kanari N, Mishra D, Gaballah I, Dupré B. Thermal decomposition of zinc carbonate hydroxide. Thermochim Acta 2004;410(1):93–100. https://doi.org/10.1016/S0040-6031(03)00396-4.
[54] Zander S, Kunkes EL, Schuster ME, Schumann J, Weinberg G, Teschner D, et al. The role of the oxide component in the development of copper composite catalysts for methanol synthesis. Angew Chem Int Ed 2013;52(25):6536–40. https://doi.org/10.1002/anie.201301419.
[55] Verrecchia EP, Verrecchia KE. Needle-fiber calcite; a critical review and a proposed classification. J Sedim Res 1994;64(3a):650–64. https://doi.org/10.1306/D4267E33-2B26-11D7-8648000102C1865D.
[56] Haynes W. CRC handbook of chemistry and physics. 93rd ed. Taylor & Francis9781439880494; 2012.
[57] Gamsjager H, Konigsberger E, Preis W. Solubilities of metal carbonates. Pure Appl Chem 2019;70:1913–20. https://doi.org/10.1351/pac199870101913.
[58] Li JL, Inui T. Characterization of precursors of methanol synthesis catalysts, copper/zinc/aluminum oxides, precipitated at different pHs and temperatures. Appl Catal A: General 1996;137(1):105–17. https://doi.org/10.1016/0926-860X(95)00284-7.
[59] Lenormand J, Salman T, Yoon RH. Hydroxamate flotation of malachite. Can Metall Q 1979;18(2):125–9. https://doi.org/10.1179/cmq.1979.18.2.125.
[60] Reddy S, Rautaray D, Sainkar SR, Sastry M. On the morphology of SrCO3 crystals grown at the interface between two immiscible liquids. Bull Mater Sci 2003;26(3):283. https://doi.org/10.1007/BF02707447.
[61] Agrawal SG, Paterson AHJ. Secondary nucleation: mechanisms and models. Chem Eng Commun 2015;202(5):698–706. https://doi.org/10.1080/00986445.2014.969369.
[62] Lee WJ, Bordoloi A, Patel J, Bhatelia T. The effect of metal additives in Cu/Zn/Al_2O_3 as a catalyst for low-pressure methanol synthesis in an oil-cooled annulus reactor. Catal Today 2019. https://doi.org/10.1016/j.cattod.2019.03.041.
[63] Chu Z, Chen H, Yu Y, Wang Q, Fang D. Surfactant-assisted preparation of Cu/ZnO/Al_2O_3 catalyst for methanol synthesis from syngas. J Mol Catal A: Chem 2013;366:48–53. https://doi.org/10.1016/j.molcata.2012.09.007.
[64] García-Trenco A, Martínez A. A rational strategy for preparing cu-zno/H-ZSM-5 hybrid catalysts with enhanced stability during the one-step conversion of syngas to dimethyl ether (DME). Appl Catal A: General 2015;493:40–9. https://doi.org/10.1016/j.apcata.2015.01.007.
[65] jing Lu P, feng Cai F, Zhang J, yu Liu Y, han Sun Y. Hydrogen production from methanol steam reforming over B-modified CuZnAlOx catalysts. J Fuel Chem Technol 2019;47(7):791–8. https://doi.org/10.1016/S1872-5813(19)30035-0.
[66] Wang L, Yang L, Zhang Y, Ding W, Chen S, Fang W, et al. Promoting effect of an aluminum emulsion on catalytic performance of Cu-based catalysts for methanol synthesis from syngas. Fuel Process Technol 2010;91(7):723–8. https://doi.org/10.1016/j.fuproc.2010.02.003.
[67] Lefebvre J, Galli F, Bianchi CL, Patience GS, Boffito DC. Experimental methods in chemical engineering: X-ray photoelectron spectroscopy-xps. Can J Chem Eng 2019. https://doi.org/10.1002/cjce.23530.
[68] Behrens M, Brennecke D, Girgsdies F, Kißner S, Trunschke A, Nasrudin N, et al. Understanding the complexity of a catalyst synthesis: Co-precipitation of mixed cu, zn, al hydroxycarbonate precursors for Cu/ZnO/Al2O3 catalysts investigated by titration experiments. Appl Catal A: General 2011;392(1):93–102. https://doi.org/10.1016/j.apcata.2010.10.031.
[69] Liu C, Guo X, Guo Q, Mao D, Yu J, Lu G. Methanol synthesis from CO2 hydrogenation over copper catalysts supported on MgO-modified TiO2. J Mol Catal A: Chem 2016;425:86–93. https://doi.org/10.1016/j.molcata.2016.09.032.
[70] Phongamwong T, Chantaprasertporn U, Witoon T, Numpilai T, Poo-arporn Y, Limphirat W, et al. CO_2 hydrogenation to methanol over CuO-ZnO-ZrO_2-SiO_2 catalysts: effects of sio_2 contents. Chem Eng J 2017;316:692–703. https://doi.org/10.1016/j.cej.2017.02.010.
[71] Li L, Mao D, Yu J, Guo X. Highly selective hydrogenation of CO_2 to methanol over CuO-ZnO-ZrO_2 catalysts prepared by a surfactant-assisted co-precipitation method. J Power Sour 2015;279:394–404. https://doi.org/10.1016/j.jpowsour.2014.12.142.
[72] Meunier N, Chauvy R, Mouhoubi S, Thomas D, Weireld GD. Alternative production of methanol from industrial CO_2. Renew Energy 2020;146:1192–203. https://doi.org/10.1016/j.renene.2019.07.010.